Dislocation pileups in small grains

Schouwenaars, R.; Kestens, L. A.I.

DOI
10.1016/j.ijplas.2023.103602

Publication date
2023

Document Version
Final published version

Published in
International Journal of Plasticity

International Journal of Plasticity 164 (2023) 103602

Contents lists available at ScienceDirect

International Journal of Plasticity

journal homepage: www.elsevier.com/locate/ijplas

Dislocation pileups in small grains

R. Schouwenaars [a,b,*], L.A.I. Kestens [b,c]

[a] Departamento de Materiales y Manufactura, Facultad de Ingenieria, Edificio O, Universidad Nacional Autonoma de Mexico. Avenida Universidad 3000, Coyoacan, Ciudad de Mexico 04510, Mexico
[b] Department of Electromechanical, Systems and Metals Engineering, Ghent University, Technologiepark 903 Zwijnaarde, Ghent 9052, Belgium
[c] Department of Materials Science and Engineering, Delft University of Technology, Mekelweg 2, CD, Delft 2628, the Netherlands

ARTICLE INFO

Keywords:
A. Dislocations
A. Grain boundaries
A. Grain size effect
B. Polycrystalline material
C. Analytic functions

ABSTRACT

While the grain size effect (GSE) is universally observed in polycrystalline metals and alloys, extended dislocation pileups (DPUs) at grain boundaries (GBs) are rarely observed. Although this discrepancy was noticed over 50 years ago, DPUs are still widely accepted as the explanation for the GSE, often expressed as the Hall-Petch (HP) relationship. To provide a quantitative assessment of the pileup hypothesis, four classical pileup models were compared to three sets of numerical calculations, spanning a grain size range from 25 nm to 25mm. To do so, the stress field and Peach-Köhler force for short dislocation segments and circular dislocation loops were calculated as closed-form expressions and simplified to the case of pileups. Published values for the Hall-Petch constant provide the reference for estimating the critical tip stress for transmission of plastic strain from one grain to its neighbour. The results are compared in terms of consistency between models and between models and experiments. Different assumptions on the pileup geometry induce important variations in the results. Tendencies found in the numerical models resemble the trends marked in compilations of experimental results; predicted values for dislocation density and plastic shear upon yielding disagree with commonly accepted values. Added to the scarceness of experimental observation, the analysis indicates that DPUs play a role in polycrystal plasticity but do not consistently explain the GSE.

1. Introduction

1.1. The grain size effect and the Hall-Petch equation

The role of grain boundaries in the plastic deformation of polycrystalline materials is most clearly demonstrated by the grain-size effect on the yield stress σ_y, which is often described by the Hall-Petch equation (Hall, 1951; Petch, 1953):

$$\sigma_y = \sigma_0 + k_{HP} d_g^{-p} \tag{1}$$

Where s_0 is the yield stress of an infinite grain, k_{HP} a fitting constant (the Hall-Petch constant) and d_g the grain diameter. The exponent $p = 1/2$ in the original equation.

The validity of Eq (1), with $p = 1/2$, has been seriously questioned (Jiang et al. 2021; Lu et al., 2022a), with the latter finding a

* Corresponding author at: Departamento de Materiales y Manufactura, Facultad de Ingenieria, Edificio O, Universidad Nacional Autonoma de Mexico. Avenida Universidad 3000, Coyoacan, Ciudad de Mexico 04510, Mexico.
E-mail address: raf_schouwenaars@yahoo.com (R. Schouwenaars).

https://doi.org/10.1016/j.ijplas.2023.103602
Received 25 November 2022; Received in revised form 6 March 2023;
Available online 28 March 2023

value for p between 0.8 and 0.9 by means of a multiscale discrete dislocation dynamics (DDD) study. Rigorous statistical analysis by Cordero et al. (2016) determined that the values of p fall into distinct populations for different alloy classes, generally with $p \neq 1/2$. Based on an extensive review of available data, Dunstan and Bushby (2013; 2014) have proposed an upper limit of $p = 1$, later refined to a $\ln(d_g)/d_g$-relationship (Li et al., 2016). The latter relationship is based on the logarithmic term in the activation stress of a dislocation source (Foreman, 1967). Dunstan and Bushby (2013; 2014) point to the problem of observer bias, i.e., the broad dissemination of the HP-relationship induces researchers to fit their results with $p = 1/2$, even if better fits can be found.

1.2. Dislocation pileups and slip propagation across the grain boundary

A widely accepted explanation for Eq. (1) is the creation of DPUs at the GBs, by assuming that plastic flow propagates through the polycrystal once the stress concentration at the tip of the pileup reaches a critical value. It is assumed that plastic strain can propagate by the bow out of a dislocation segment from the first grain into the second one (Shen et al., 1988; Clark et al., 1992; Bieler et al., 2014; Zhang et al., 2021; Aragon et al., 2022; Bamney et al., 2022) or by the activation of dislocation sources inside the second grain (Liu et al., 2020). Recent reviews on the experimental evidence and large-scale simulation of grain boundary – dislocation interactions were provided in connection with the study of dislocation emission from GBs (Schouwenaars, 2020; Zhang et al., 2020) and dislocation transmission at GBs (Kacher et al., 2014; Bayerschen et al., 2016).

Dislocation transmission has been successfully incorporated in DDD models for polycrystals (Zhang et al., 2021; Lu et al., 2022a, 2022b). Trapping and emission of dislocations was studied with DDD by Bamney et al. (2021). It shall be noted that in none of these studies, the concept of DPUs is incorporated to promote bow-out of dislocations into the next grain. Instead, the GSE is induced by the stress field of dislocations stored at or near the GB by stochastic processes.

To study DPUs in micromechanical models, they must be introduced explicitly, as was done by Guan et al. (2019) in the analysis of the texture dependence of k_{HP} in Mg. These authors also stress the relative importance of micro- and macro-strains for k_{HP} in Ti, as assessed by a crystal plasticity finite element model (CPFEM) (Guan et al., 2022). A multiscale model studying the details of the interaction between the DPU and GB was proposed by Peng et al. (2022), who demonstrated the importance of the structural modification of the GB by dislocation absorption and transmission.

1.3. Alternative explanations for the GSE

Various alternative explanations for the GSE were reviewed into detail by Cordero et al. (2016), who provided a broad review of available models and an extended compilation of experimental data. The slip length argument (Conrad 1963; Saada, 2005), combines the Taylor equation (Taylor, 1934) with the Orowan equation (Orowan, 1940) under the assumption that the slip length in the latter equation is proportional to the grain size. This produces a $d_g^{-1/2}$ relationship.

The hypothesis that the release of GB-boundary ledges into the grain induces yielding was proposed by Li and Chou (1970) and reviewed by Li et al. (2020). A $d_g^{-1/2}$ relationship is again found. The observation that GB-ledges are donors, not sources for dislocations (Varin et al., 1987) is not inconsistent with this hypothesis, but the high stress associated to the activation of this mechanism may limit its validity to submicrometric grains (Schouwenaars, 2020).

Source length arguments based on Foreman's equation for dislocation bow-out (Foreman, 1967; Ovid'Ko et al., 2018), predict a $d_g^{-1}\log d_g$-relationship, which is retained in refinements of this equation based on a statistical analysis of GB-dislocation sources (Kato et al., 2008; Yuan et al., 2015, 2016). The $d_g^{-1}\log d_g$-relationship disappears in the statistical analysis of bulk sources developed by El-Awady (2015) and Gu et al. (2021), who found that fitting values for p depend strongly on the assumptions about the probability distribution of the source lengths.

Ashby (1970) introduced geometrically necessary dislocations to accommodate the misfit induced by the strain incompatibility between elastically anisotropic grains. This model is closely related the core-shell model (Meyers et al., 2006) which invoke the same incompatibility to justify the existence of an outer shell of higher dislocation density near the grain boundary. Both approaches provide a $d_g^{-1/2}$-relationship but do not identify the sources of these dislocations nor the slip caused by their emplacement.

1.4. Advanced numerical models

Micromechanical models provide a more precise assessment of the plastic deformation and dislocation behaviour associated to strain incompatibilities. Berbenni et al. (2020) used a fast Fourier transform elasto-viscoplastic model to study the increased dislocation densities at grain boundaries. This was also achieved by Jiang et al. (2019; 2021), who studied the behaviour of a grain with impenetrable GBs embedded in an elastic medium by DDD. Continuum dislocation dynamics has been used to simulate the dislocation distributions predicted by core-shell models (Kalaei et al., 2022), which have recently been backed-up by electron backscattering diffraction (Pai et al., 2022). The combined use of DDD and CPFEM provides additional information for core-shell type models in polycrystals (Jiang et al., 2022; Zhang et al., 2022), as is the case for a dislocation density-based hardening model incorporated into CPFEM for an Al-oligocrystal (Demir and Gutierrez-Urrutia, 2021).

A disadvantage of DDD, CPFEM and multiscale models is their computational cost, which limits the results to small grains and often does not allow a systematic study of all parameters involved. Simplified or theoretical models for dislocation interaction lack the detail and sophistication of advanced simulations but add flexibility in terms of the number and range of parameters that can be included.

1.5. Theoretical analysis of DPUs

This work focuses on the DPU-hypothesis alone. A textbook explanation of the general problem is given by Hirth and Lothe (1992). An extensive overview of the early work in the field is provided by Li and Chou (1970). Specific results required for the elaboration of this work will be cited in the corresponding sections.

More recent models for DPUs have analysed the effect of the source length (Friedman and Chrzan, 1998) and DPUs affected by stress gradients (Akarapu and Hirth, 2013), or both (Szajewski et al., 2013; Zamani et al., 2015). These studies illustrate the ongoing scientific interest in the topic but do not alter the general conclusions on the role of DPUs in relationship to the GSE. The interaction between a pileup and a disclination was studied by Rybin et al. (2018) and Perevezentsev et al. (2020). These simplified models incorporate the strain-induced GB-deformation which was studied with an advanced multiscale model by Peng et al. (2022). Liu et al. (2022a) studied the effect of DPUs at grain boundaries with varying strength in a study of the Bauschinger effect. Anisotropic bicrystals were analysed by Wagoner (1981) and pileups in multiphase anisotropic materials were investigated by Chen et al. (2019; 2021).

The effect of multiple pileups at a single GB has been studied by considering the equilibrium position of a set of infinite arrays of equidistant dislocations (Roy et al., 2008; De Geus et al., 2013). Strictly spoken, this approach models the pileup of low-angle GBs against a high-angle GB. Scardia et al. (2014) demonstrated that the distance distribution between the dislocation arrays is strongly dependant on the distribution of the dislocations within the arrays and the pileup. Baskaran et al. (2010) reached a similar conclusion and emphasized that the angle between the DPUs and the GB strongly influences the equilibrium positions of the dislocation arrays, with the perpendicular case corresponding to a singularity. Both studies illustrate how small modifications in the initial assumptions can cause significant modifications in the results of DPU-models. Schouwenaars et al. (2010) concluded that a random distribution of the number of dislocations in each pileup and random distribution of parallel pileups along the GB, as can be expected in real-world polycrystals, eliminates any direct connection to Eq. (1).

1.6. Experimental evidence of DPUs

Bailey and Hirsch (1960) rejected DPUs as an explanation for the GSE based on transmission electron microscopy observations (TEM) and calorimetric measurements. Li and Chou (1970) rejected a direct connection to the GSE due to the scarcity of experimental observations of DPUs, an argument repeated by Saada (2005). Murr (2016) is more precise in this assessment, by reviewing the generalised presence of well-defined DPUs in stainless steel (a low stacking fault alloy) as compared to their absence in Cu and Ni (medium stacking fault metals). Li et al. (2020) point out the irony of the fact that the DPU-mechanism was first invoked for iron and steel (Petch, 1953; Hall, 1951), but that DPUs are seldomly observed in dilute iron alloys.

DPUs are generally studied by TEM. Chassaigne et al. (2011) found evidence of short DPUs at twin boundaries in Cu. Zhou et al. (2019) studied dislocation transmission at Cu-Brass interfaces and present an image of a pileup consisting of 5 dislocations. They confirm that this is an exception and most of the dislocation transmission is preceded by the formation of complex dislocation entanglements, as was concluded by Murr (2016) as well. Parallel short DPUs (up to 7 dislocations) were found in Inconel by Zhao et al. (2020) and in 316H stainless steel by Li et al. (2021). In both papers, complex dislocation entanglements at GBs were more common than DPUs. More extensive DPUs were found in an ATI 718 superalloy (Liu et al., 2022a). Slip bands observed by high resolution electron backscattered diffraction (HR-EBSD) provide evidence that in titanium, the DPUs show good coincidence with the theoretical predictions (Britton and Wilkinson, 2012; Guo et al., 2014).

A particular class of observations is associated to *in-situ* nanoindentation experiments (Soer et al., 2004; De Hosson et al., 2006; Kondo et al., 2016; Piao and Khanh, 2021). Here, the indentation serves as a localised source of dislocations. Pileups against nearby grain boundaries are generally observed. Ruggles et al. (2020) combined nanoindentation with HR-EBSD to analyse DPUs in Tantalum. DPUs formed against precipitates in a Mg-RE alloy were found to be significantly more complex than predicted by basic theory, due to the tortuous path imposed by the restricting second phase particles (Huang et al., 2019). Non-standard behaviour was also found for the interaction between a pileup and twin boundary in nickel as analysed by Li et al. (2022). In first instance, the DPU was reflected; limited transmission from multiple sources only occurred after the formation of dislocation entanglements. DPUs, as well as extensive dislocation absorption and emission was seen in the compression of bicrystal nanopillars by Chen et al. (2020). Multiple DPUs were observed in the compression of a lamellar α-β Ti nanopillar, but comparison to theoretical models is complicated due to the complex geometry of the sample (Zheng et al., 2018).

In summary, DPUs are observed if they are purposely induced by specific experiments. This allows to study their interaction with GBs under controlled conditions. Except for low stacking fault energy materials, DPUs are rare under normal loading conditions. If they are found, they contain only a few dislocations. There seems to be no experimental confirmation of the correlation between the grain size and the length of the observed DPUs.

1.7. Outline

The work starts from the widely accepted hypothesis that DPUs are responsible for the GSE. Then, following the method of proof by contradiction, if the results of the calculations are inconsistent with the starting hypothesis, it must be rejected, or at least be seriously questioned. Except for data from detailed TEM-observation, the measurable quantity which can be used to calibrate pileup models is the exponent p and constant k_{HP} obtained from extensive literature reviews (Cordero et al., 2016). Given k_{HP}, the relationship between d_g and the critical pileup tip stress τ_c can be calculated for a given number n of dislocations in the pileup. Section 2 will provide a summary of the commonly used pileup models. Section 3 will elaborate the stress fields and Peach-Köhler force for short, straight

dislocation segments and for circular dislocations in a general form. The general result is then simplified to obtain the average Peach-Köhler force between slip dislocations in the plane of the pileup.

Section 4 outlines the essential aspects of the numerical solution of the set of nonlinear equations which describe the equilibrium of the Peach-Köhler force and the self-stress. Numerical results are compared to the analytical expressions and between each other. The plastic deformation associated to the formation of the pileups and the corresponding dislocation density are calculated and compared to conventionally accepted values.

2. The classical pileup models

2.1. Preliminary considerations

To write all formulas in non-dimensional form, lengths will be expressed as multiples of the magnitude b of the Burgers vector and stresses as multiples of the shear modulus m. Calculations assume isotropic linear elasticity. Scalars are presented as italic-face letters, vectors as bold face. The Burgers vector $\mathbf{b}$ is a unit vector in this notation, as is $\boldsymbol{\xi}$, the tangent vector to the dislocation line. The dyadic product ($\otimes$) is not used, instead, the outer product or tensorial product is written without symbol, e.g., $\mathbf{b}\boldsymbol{\xi}$ is a second rank tensor with components $b_i\xi_j$.

For a dislocation blocked by a GB, $\boldsymbol{\xi}$ is determined by the intersection between the slip plane and the GB-plane, hence the limiting cases of pure edge or pure screw dislocations will almost never occur. The non-dimensional pre-factor for the stress formulae for general straight dislocation segments is given as (Li and Chou, 1970):

$$A = \frac{1}{2\pi(1-\nu)}\left(\sin^2\psi + (1-\nu)\cos^2\psi\right) \tag{2}$$

where ψ is the angle between $\mathbf{b}$ and $\boldsymbol{\xi}$. The expected value for A, averaged over all ψ, is given by Schouwenaars (2020):

$$\langle A\rangle = \frac{(2-\nu)}{4\pi(1-\nu)} \tag{3}$$

Coincidently, this is also the value obtained for $\psi=\pi/4$. The value of $\langle A\rangle$ is only needed to plot results. In the few cases where conventional length and stress units are preferrable, the Burgers vector ($b = 0.256\ 10^{-}9$ m) and shear modulus (μ=58.1 10^9 Pa) for Cu will be used. Poisson's ratio cannot be hidden by using dimensionless expressions and will be set equal to its value in Cu (ν=0.34). Uniaxial strain ε will be converted into shear strain g by using an approximate Taylor factor $M = 3$ (i.e., $\gamma=M\varepsilon$) and the critical resolved shear stress at yield $\tau_y=\sigma_y/M$. This is done to follow conventional practice (Argon, 2007), although it may be argued that a Schmid factor is more appropriate at the onset of plastic deformation if the process is ruled by pileup formation on a single slip system (Demir et al., 2021).

The relationship between DPUs and the GSE assumes that there exists a critical shear stress τ_c at which plastic strain is transmitted from one grain to its neighbour. For each of the existing models, a relationship can be obtained between k_{HP} and τ_c (Li and Chou, 1970). Taking Cu as the example, k_{HP} ≈110 000 Pa$\sqrt{\text{m}}$ (Cordero et al., 2016) or 0.118 in non-dimensional units. The three configurations

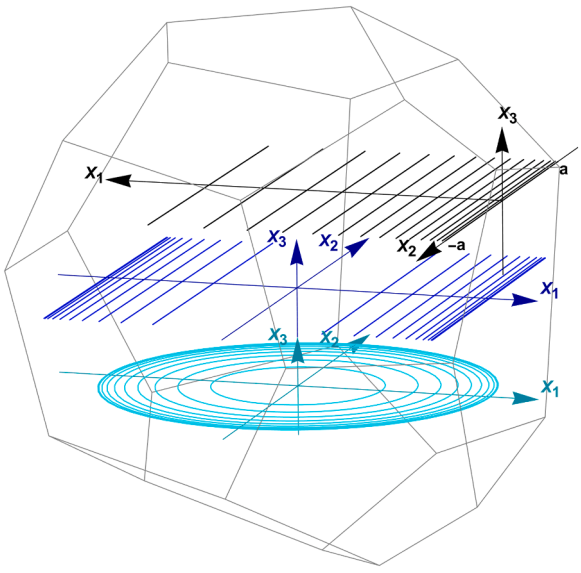

Fig. 1. Three pileup configurations: the single pileup of short straight dislocations (SPSD) is shown in black, the double pileup of short straight dislocations (DPSD) in blue and the discrete pileup of circular dislocations (DPCD) in cyan.

(single pileup, double pileup, and pileup of circular dislocation loops) are summarised in Fig. 1.

2.2. Single pileup of infinite straight dislocations (SPID)

Under an applied shear stress τ, the equilibrium equations for n dislocations are given as (Chou, 1967):

$$\frac{kA}{x_j} + \sum_{i=1, i\neq j}^{n-1} \frac{A}{x_j - x_i} - \tau = 0 \; j: 1 \rightarrow n-1 \tag{4}$$

Here, the grain boundary is at $x = 0$ and contains a pinned dislocation with Burgers vector kb. The factor k introduces a certain degree of flexibility, as the GB-dislocation may have different strength than the dislocations in the slip plane, at positions x_i. For $k = 1$, the original Eshelby-Frank-Nabarro (EFN) problem is recovered (Eshelby et al., 1951). Defining the roots of the generalised Laguerre polynomial $L_n^{2k-1}(x)$ as r_i, it is found that the $x_i = Ar_i/2t$.

In the continuum approach (Leibfried, 1951; Head and Louat, 1955; Hirth and Lothe, 1992) (HL), the individual positions of the dislocations are substituted by a continuous distribution $n(x)$ of infinitesimal dislocations and the summation in Eq. (4) becomes an integral:

$$A \int_0^a \frac{n(x')}{x - x'} dx' = \tau \tag{5}$$

Solving Eq. (5) yields:

$$n(x) = \frac{\tau}{\pi A} \sqrt{\frac{a - x}{x}} \tag{6}$$

It is seen that a corresponds to the point where $n(x)$ becomes equal to 0. Normally it is assumed that $a = d_g$. The tip stress is given by $\tau_{Tip} = n\tau$. It is assumed that yield propagates through the polycrystal at a critical tip stress t_c:

$$\tau_c = n\tau_y \tag{7}$$

and the relationship between n, τ_y and d_g is found as:

$$d_g = \frac{2nA}{\tau_y} \tag{8}$$

By eliminating n from Eq. (7) using Eq. (8), it is found that:

$$\tau_y = \sqrt{\frac{2A\tau_c}{d_g}} \tag{9}$$

Comparison to Eq. (1) identifies Eq. (9) as the second term in HP and allows concluding:

$$k_{HP} = \sqrt{2A\tau_c} \tag{10}$$

Which, under the SPID-approach, allows calculating τ_c from experimentally obtained values of k_{HP}. A useful relation is found by eliminating τ_c and τ_y from Eq. (9) by means of Eqs. (10) and (7):

$$d_g = \frac{4n^2A^2}{k_{HP}^2} \tag{11}$$

This allows calculating d_g from n. Together with (9), a τ_y-d_g plot can be constructed for all values of n. Such a plot is required to make the comparison with numerical values which are obtained for each value of n separately.

To compare the EFN-solution to the continuum solution and numerical results, discrete positions for the dislocations must be calculated. This can be done by integrating $n(x)$ on the interval $[0, x_m]$, where x_m corresponds to the position of the $m + 1^{\text{th}}$ dislocation, counted from the blocked dislocation at the GB. The following equation must be solved:

$$m = \frac{k_{HP}}{\pi A \sqrt{d_g}} \int_0^{x_m} \sqrt{\frac{d_g - x}{x}} dx \tag{12}$$

After integration it is found that:

$$m = \frac{2n}{\pi A} \left(\arctan \sqrt{\frac{d_g}{x_m} - x_m} - \sqrt{x_m \left(1 - \frac{x_m}{d_g} \right)} \right) \tag{13}$$

This transcendental equation must be solved numerically.

2.3. Double pileup of infinite straight dislocations (DPID) and continuum approach for the pileup of circular dislocation loops (CPCD)

An analytical solution such as EFN is not known for these configurations. Following the steps outlined for SPID, the continuum approximation yields the following results for the DPID (Li and Chou, 1970; Hirth and Lothe, 1992):

$$k_{HP} = 2\sqrt{2A\tau_c} \tag{14}$$

and:

$$d_g = \frac{4\pi^2 A^2 n^2}{k_{HP}^2} \tag{15}$$

The positions of the individual dislocations are found as shown in Section 2.2:

$$x_m = \pm a\sqrt{\frac{m}{n}}\sqrt{2-\frac{m}{n}} \tag{16}$$

The CPCD-model neglects the self-stress of the loops as well as the dependence of the stress field on the angle ψ. The essential results are (Li and Chou, 1970):

$$k_{HP} = \sqrt{\frac{\pi(2-\nu)\tau_c}{2(1-\nu)}} \tag{17}$$

It is also found that:

$$d_g = \frac{\pi^2(2-\nu)^2 n^2}{16(1-\nu)^2 k_{HP}^2} \tag{18}$$

The radius of the corresponding discrete dislocation loops is given by Eq. (16). To compare the circular loops to the straight segments, the average value $\langle A\rangle$ Eq. (3)) will be used, which has the same dependence on n as found in Eqs. (17) and ((18). Notice that d_g=2a for double pileups and circular dislocations.

3. Theoretical development

3.1. Methodology

The stress field due to the presence of a dislocation is given by the following line integral (Peach and Köhler, 1950; Hirth and Lothe, 1992):

$$\boldsymbol{\sigma} = -\frac{1}{4\pi}\oint_C\left(\mathbf{b}\times\ \nabla\frac{1}{R}\right)\mathbf{dl} - \frac{\mu}{4\pi}\oint_C \mathbf{dl}\left(\mathbf{b}\times\ \nabla\frac{1}{R}\right) - \frac{1}{4\pi(1-\nu)}\oint_C \nabla\left(\nabla\nabla R - I\nabla^2 R\right)\cdot(\mathbf{b}\times\mathbf{dl}) \tag{19}$$

with:

$$R = \sqrt{(x_1 - x'_1)^2 + (x_2 - x'_2)^2 + (x_3 - x'_3)^2} \tag{20}$$

C is the curve describing the dislocation and **dl** an infinitesimal tangent vector to C. **I** is the second rank unit tensor. **x** is the coordinate of the points on C and **x**' the coordinate in space where the stress tensor is evaluated. Derivatives are taken with respect to **x**'. The Peach-Köhler force acting on a dislocation segment with Burgers vector **b** and tangent vector **x** is given by:

$$\mathbf{F_{PK}} = (\mathbf{b}\cdot\boldsymbol{\sigma})\times\boldsymbol{\xi} \tag{21}$$

Eq. (19) is slightly adapted from the notation used by Hirth and Lothe (1992) and was checked against the formula expressed in index notation in the same reference. The tensor form has the advantage that it can be programmed in a compact and straightforward manner using mathematical software. The fundamental step in elaborating Eq. (19) is to write C in parametric form, choosing a reference system that allows simplifying the tensors as much as possible. The result can then be used in any reference system using standard rules for the transformation of tensor components under coordinate transform.

Elaboration of the derivatives in Eq. (19) is laborious; integration is generally difficult, even for very simple configurations, and often involves non-elementary functions. Therefore, the procedure was formalised using mathematical software (see supplementary information A and B). This allows for the elaboration of all tensors and symbolic integration over suitably defined paths C. All human manipulation of the formulas was avoided, i.e., the common practice of identifying recurring groups of expressions by new symbols was not followed. This leads to less elegant expressions but avoids errors due to copying and substitution of parts of complex formulas.

For pileups of finite straight dislocation segments or circular loops, $\mathbf{F_{PK}}$ varies along the dislocation line. If such dislocations were free to glide, they would change their shape due to the stress field of neighbouring dislocations or self-stress. This effect is neglected in the calculations; the equilibrium position is calculated using the average Peach-Köhler force along the line or curve. Incorporation of

this changing curvature or the waviness of dislocations due to interaction with solutes (Ji et al., 2020, 2022) would considerably complicate the analysis and may even be impossible with the analytical approach used here. The results (stress field, force field and average force) are implemented as user-defined functions for the purpose of plotting and for equilibrium calculations.

3.2. Stress fields and mean Peach-Köhler force of finite straight dislocation segments

The complete stress tensor was calculated for a dislocation segment spanning from $-w$ to w on the X_2-axis, with general Burgers vector **b** (see supplementary information A; notice that the commercial software Mathematica® is required to open the file). Hence, the length of the dislocation segment is $2w$, expressed in multiples of Burgers vector lengths. Combined with Eq. (21), this result allows calculating the interaction between non-collinear dislocations of edge, screw and climb character. It shall be noted that this problem was already treated by Kroupa (1961), Hirth and Lothe (1992), but recalculating the results with the help of mathematical software is faster than manually copying the original result into such software. A graphical representation of the stress field for an edge dislocation is given in Fig. 2. The stress singularity for σ_{23} at the endpoints of the segments is very localised, showing that end effects are indeed

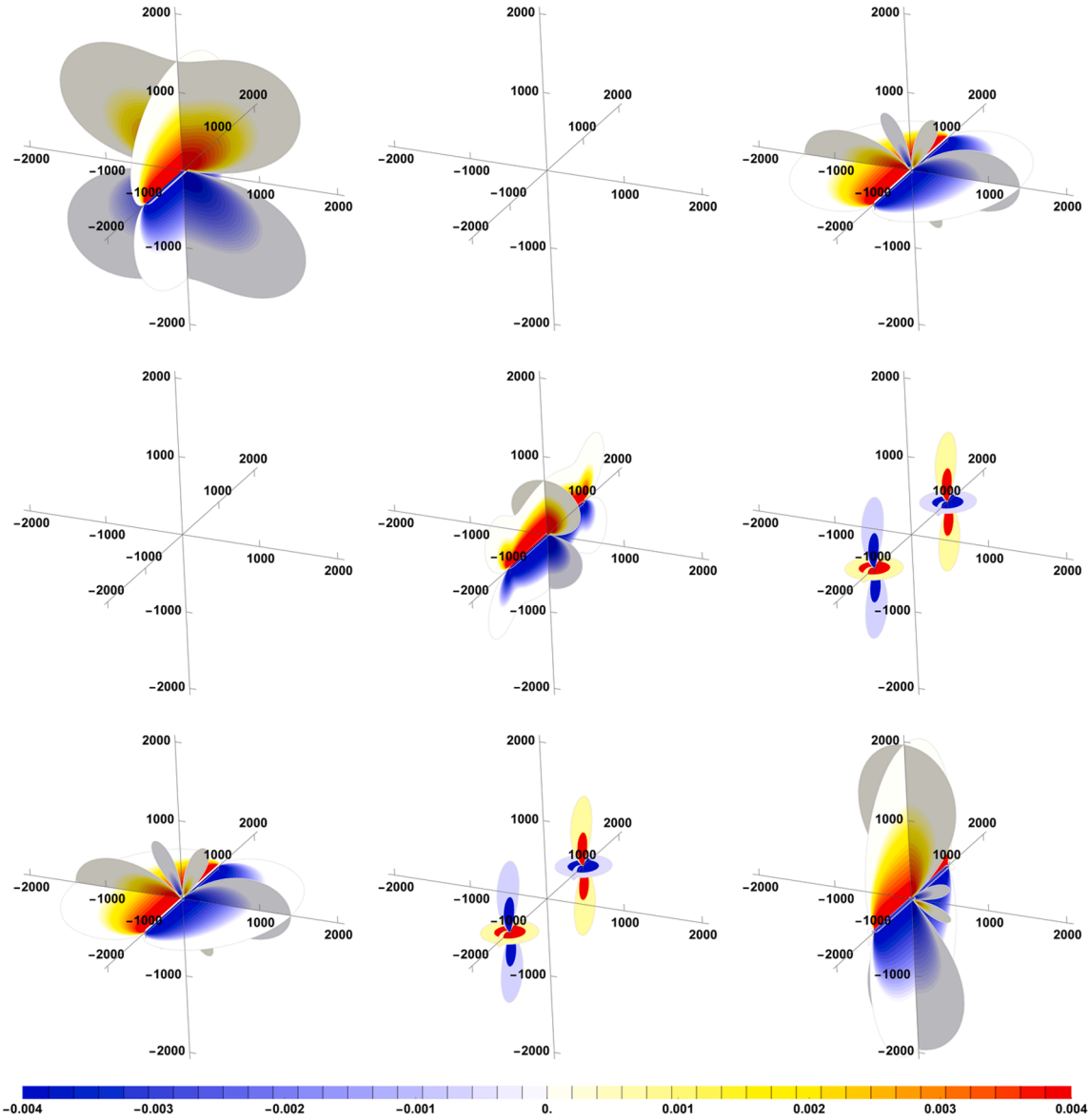

Fig. 2. Graphical representation of the stress tensor of an edge dislocation segment of $2w = 2000$ (non-dimensional units). Axis coordinates represent non-dimensional distance, colour codes show non-dimensional stress. The position in the image of each plot corresponds to the position of each component in **σ**. Notice the localised stress singularity for σ_{23} at the ends of the segment.

small (Hirth and Lothe, 1992).

To study the interactions between short, parallel glide dislocations with the same **b**, the general expression $\mathbf{F_{PK}}$ can be simplified significantly. For a segment along the X_2-axis centred at (x_1,0,0) acting on a coplanar parallel segment at (x'_1,0,0), the glide component becomes:

$$F_{PK_1} = A\frac{x_1x_2\left(\sqrt{x_1^2+(w-x_2)^2+x_3^2}-\sqrt{x_1^2+(w+x_2)^2+x_3^2}\right)+x_1w\left(\sqrt{x_1^2+(w-x_2)^2+x_3^2}+\sqrt{x_1^2+(w+x_2)^2+x_3^2}\right)}{2(x_1^2+x_3^2)\sqrt{x_1^2+(w-x_2)^2+x_3^2}\sqrt{x_1^2+(w+x_2)^2+x_3^2}} \tag{22}$$

The average force from a segment is found by integrating $\mathbf{F_{PK}}$ over x_2 from -w to w and dividing by 2w:

$$\overline{F_{PK_1}} = A\frac{4w^2+(x_1-x'_1)^2-\sqrt{4w^2(x_1-x'_1)^2+(x_1-x'_1)^4}}{2w(x_1-x'_1)\sqrt{4w^2+(x_1-x'_1)^2}} \tag{23}$$

By taking the limit for $w\to\infty$, this simplifies to:

$$F^{\infty}_{PK_1} = \frac{A}{(x_1-x'_1)} \tag{24}$$

which was used in Eq. (4). It is seen that even though the end effects are highly localised (Fig. 2), the length of the segment has a strong influence on $\overline{F_{PK_1}}$.

3.3. Stress fields and mean Peach-Köhler force of circular dislocation loops

A numerical analysis of the pileup of circular dislocation loops was performed first by Li and Liu (1967). The latter work cites unpublished calculations by one of the authors, so it is not possible to trace the simplifications used in this early paper. Khraishi et al., 2000a; 2000b) presented an extensive review of early attempts to solve the problem of circular dislocation loops, which are characterised by a long history of calculation errors. The study of prismatic loops is particularly important in the framework of irradiation damage in nuclear materials (Khraishi et al., 2000a; Zhang et al., 2018).

Khraishi et al., 2000a) calculated the stress field using the Burgers displacement equation (Hirth and Lothe, 1992). They employed mathematical software to elaborate the integrals and present the solutions in compact form by defining new symbols for recurring expressions in the equations. Deformations were determined by deriving the displacement field and stresses by means of Hooke's law. In a second paper (Khraishi et al. 2000 b), direct integration of the Peach-Köhler equation is presented. Many intermediate results were omitted from the publications, which complicates a reproduction of the original method.

Therefore, the calculations were repeated from zero for the present work and are provided as supplementary material (Supplementary information B; notice that the commercial software Mathematica® is required to open the file). Even though modern mathematical software has amazing capabilities in terms of symbolic calculations, the problem must be reduced to its simplest possible form to obtain usable results, without reducing generality.

The basic geometry is shown in Fig. 3. The calculations are performed in Cartesian coordinates for the three components of the Burgers vector separately. Superposition is used to obtain the result for any Burgers vector. The calculations are only performed in the

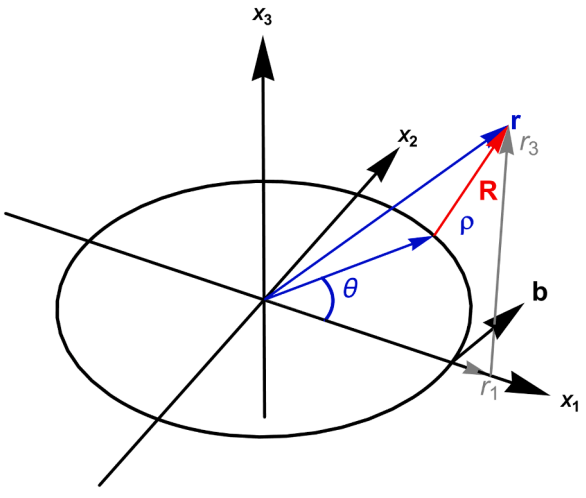

Fig. 3. Coordinate system used for the calculation of the stress field. $\mathbf{r}_1$ defines a vector on the loop with coordinates ($r_1\cos\theta$, $r_1\sin\theta$, 0), $\mathbf{r}_2$ is any vector in the x_2=0 plane, $\boldsymbol{R} = \mathbf{r}_2$-$\mathbf{r}_1$. The integrals Eq. (25) are performed over θ. **b** can be any unit vector.

x_2=0 plane. Rotating **b** clockwise over an angle ϕ with respect to the X_3-axis then corresponds to a counter-clockwise rotation of the x_2=0 plane for a constant **b**, producing the complete solution in cylindrical coordinates. The integrals in Eq. (19) can be performed by defining C as ($r_1\cos\phi$, $r_1\sin\phi$, 0) and integrating over ϕ from -π to π. To illustrate the results of the general calculations, an example plot for the stress field is given in Fig. 4 for **b** parallel to X_1.

Care must be taken when calculating $\mathbf{F_{PK}}$, as the stress field $\mathbf{s^{Cyl}}$ is given in cylindrical coordinates. Defining the rotation matrix with respect to the X_3 axis over an angle ϕ as $\mathbf{R}_3(\phi)$, $\mathbf{F_{PK}}$ is obtained in cylindrical coordinates by:

$$\mathbf{F}_{\mathbf{PK}}^{\mathbf{Cyl}} = \mathbf{R}_3(\phi) \cdot \left(\left(\mathbf{b} \cdot \mathbf{R}_3^{\mathbf{T}}(\phi) \cdot \boldsymbol{\sigma}^{\mathbf{Cyl}} \cdot \mathbf{R}_3(\phi) \right) \times \boldsymbol{\xi} \right) \tag{25}$$

For **b** parallel to X_1, only the radial component $F_{PK_r}^{Cyl}$ is distinct from 0.

$$F_{PK_r}^{Cyl} = \frac{\nu\left(2r_1^2 + r_2^2\right)\cos(2\phi)\mathrm{K}\left(-\frac{4r_1r_2}{(r_1-r_2)^2}\right) - (2-\nu)r_2^2}{4\pi(1-\nu)r_2^2(r_1-r_2)} - \frac{\nu\left(2r_1^2 + r_2^2\right)\cos(2\phi)\mathrm{E}\left(-\frac{4r_1r_2}{(r_1-r_2)^2}\right) + (2-\nu)r_2^2}{4\pi(1-\nu)r_2^2(r_1+r_2)} \tag{26}$$

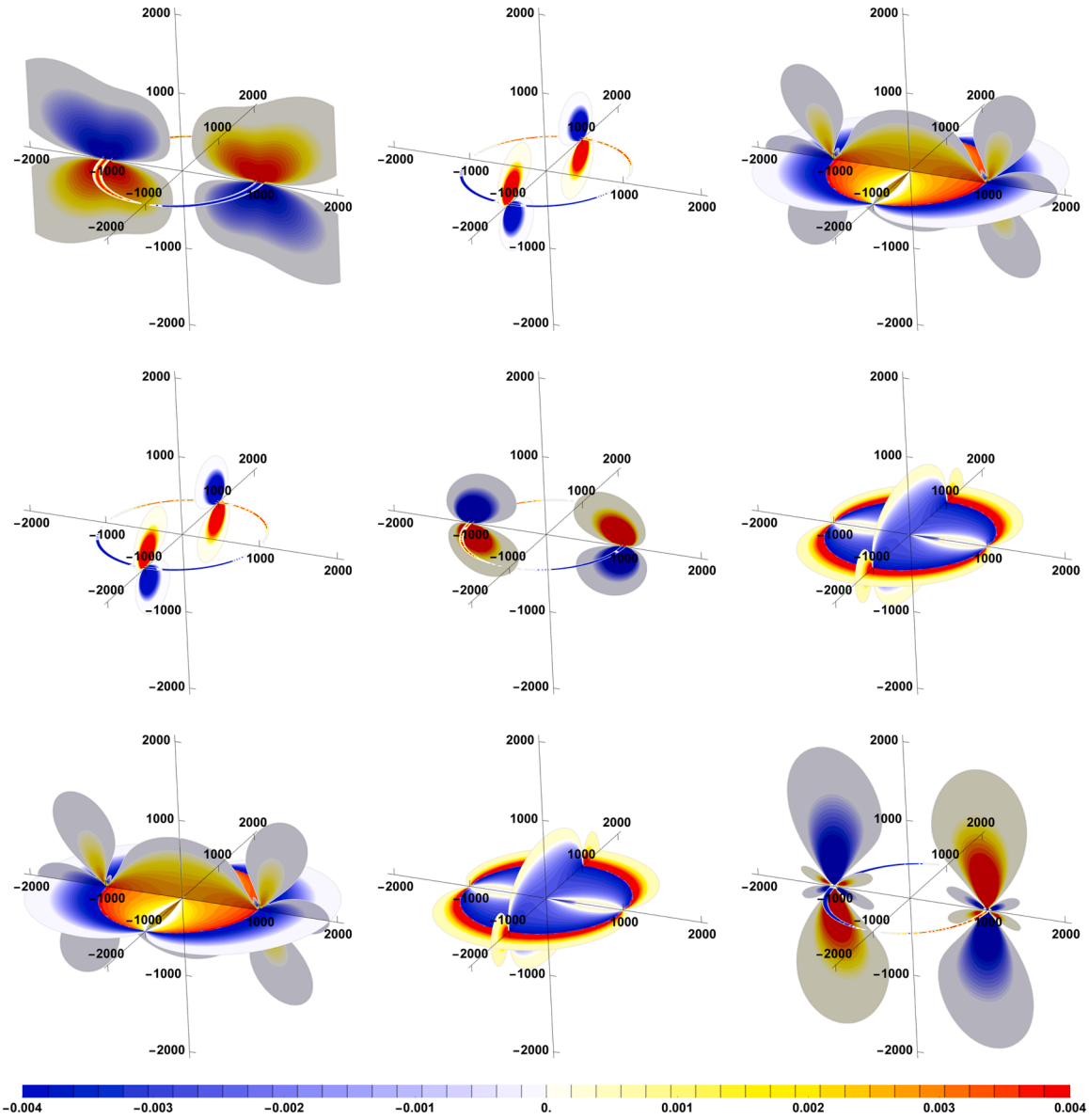

Fig. 4. Graphical representation of the stress tensor of a glide dislocation loop with radius 1000 (non-dimensional units). Axis coordinates represent non-dimensional distance, colour codes show non-dimensional stress. The position in the image of each plot corresponds to the position of each component in **σ**.

Here, K(·) and E(·) are the complete elliptic integrals of the first and second kind. The angular dependence of $F_{PK_r}^{Cyl}$ reflects the fact that the equilibrium shape of a dislocation loop in an isotropic medium is elliptic. The case of circular loops is a simplification. Averaging over ϕ produces:

$$\overline{F_{PK_r}^{Cyl}} = \mathrm{sign}(r_1 - r_2)\frac{(2-\nu)\left((r_1-r_2)\mathrm{E}\left(-\frac{4r_1r_2}{(r_1-r_2)^2}\right)+(r_1+r_2)\mathrm{K}\left(-\frac{4r_1r_2}{(r_1-r_2)^2}\right)\right)}{4\pi(1-\nu)(r_1-r_2)^2} \tag{27}$$

To calculate the self-stress of the loop, the integrands in Eq. (19) were recalculated by taking limits for $r_2 \to r_1$ and repeating the procedure described to calculate the stress field. The integrals are non-converging at θ=0, so the integrals are calculated over [-π,-δ/2] and [δ/2,π], with δ a cut-off angle which relates to the more commonly used cut-off radius $r_0 = r_1\delta$. As an example of the limiting procedure, the result is given for **b** parallel to X_1 and ϕ=0. In this case, only σ_{13} is distinct from 0:

$$\sigma_{13} = -\frac{1}{4\pi}\frac{2\cos\left(\frac{\delta}{4}\right)+\ln\left(\tan\left(\frac{\delta}{8}\right)\right)}{r_1^2}+\frac{1}{4\pi(1-\nu)}\frac{2\cos\left(\frac{\delta}{4}\right)-\ln\left(\cot\left(\frac{\delta}{8}\right)\right)}{r_1^2} \tag{28}$$

To express this equation in terms of r_0, it must be noted that, for small δ:

$$\delta \to 0 : \cos\left(\frac{\delta}{4}\right)\to 1;\ \tan\left(\frac{\delta}{8}\right)\to\frac{\delta}{8};\ \cot\left(\frac{\delta}{8}\right)\to\frac{8}{\delta} \tag{29}$$

This allows rewriting Eq. (28) as:

$$\sigma_{13} = -\frac{(1-2\nu)}{4\pi(1-\nu)}\left(\ln\left(\frac{8r}{r_0}\right)-1\right) \tag{30}$$

The substitutions (Eq. (29)) can be performed automatically using mathematical software for all components of **b** and **σ**. The self-force is calculated with Eq. (25) and depends on the angle ϕ (see supplementary material B). The average self-force in radial direction is given by:

$$\overline{F_{PK_S}} = -\frac{(2-\nu)\ln\left(\frac{8r_1}{r_0}\right)}{8\pi(1-\nu)r_1} \tag{31}$$

Fig. 5. compares Eqs. (27) and (31) to the formulas used by Li and Liu (1967). The differences are small, except for the force exercised by a loop on a smaller loop.

4. Numerical simulation and comparison to classical models

4.1. Methodology

The numerical determination of the equilibrium positions for the dislocation configurations shown in Fig. 1 requires the solution of a system of n nonlinear equations as in Eq. (4). Independent of the specific geometry studied, the interaction force F_{ij} between dislocations i and j is written as:

$$F_{ij} = \begin{cases} F_{PK}(x_j - x_i) & i \neq j \\ F_s(x_i) & i = j \end{cases} \tag{32}$$

where x_i and x_j denote the position on the X_1 axis for straight dislocations or the radius for circular loops.

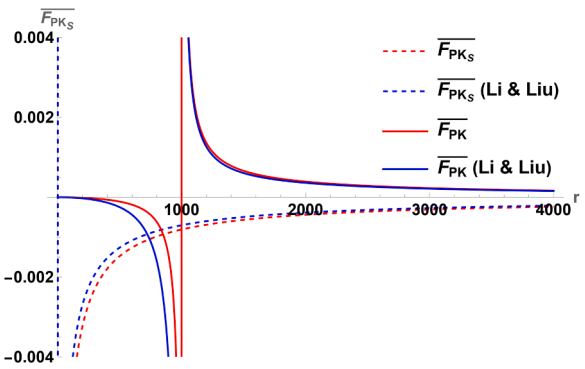

Fig. 5. Comparison between the present results and the equations used by Li and Liu (1967). The full curves describe the interaction between a loop with r_1=1000 and a second loop with radius r. The dashed curves show the self-force of a loop with radius r.

For the SPSD, F_{PK} is equal to $\overline{F_{PK_1}}$ in Eq. (23) and the self-force F_S is equal to 0. The variable w can be modified freely, and a value of $w = 0$ is used as a flag for using Eq. (24) instead of Eq (23), i.e., to study infinite dislocations.

For the DPSD, F_{PK} in Eq. (32) is set equal to the mean Peach-Köhler force of a dislocation dipole at x_i and -x_i, i.e., $F_{PK}(x_j - x_i) = \overline{F_{PK_1}}(x_j - x_i) - \overline{F_{PK_1}}(x_j + x_i)$, due to the symmetry of the configuration. The self-force $F_S(x_i)$ corresponds to the interaction between the positive dislocation at x_i the negative one -x_i. For the DPCD, Eqs. (27) and (31) are used for F_{PK} and F_S respectively.

For the SPSD, the number of simulations is reduced by considering that only the dislocation configuration which achieves $\tau_{Tip}=\tau_c$ is of interest. This introduces an additional equation into the system, stating that the sum of the F_{PK} plus the applied shear stress τ is equal to τ_c for the dislocation locked at the GB. Then, the input data are the dislocation width w, the number of dislocations n and the critical tip stress τ_c. The output are the positions x_i of the dislocations and the applied stress τ_y at the moment of slip transmission. The position x_n of the n^{th} dislocation defines the grain diameter. An additional set of simulations was performed, where w was left free and the condition $2w=x_n$ was introduced as an additional equation. This corresponds to a configuration where the length of the pileup is equal to the length of the dislocation segments. Starting values for solving the $n \times n$ system were calculated from Eq. (13), using $A = \langle A \rangle$.

In DPSD, d_g is determined by a fixed dislocation at the GB, which is placed at $d_g/2$. The condition $2w=d_g$ was imposed. For DPCD, $d_g=2a$ and is determined by a fixed dislocation with radius a. For both geometries, n and τ_c do not completely define the configuration. For a given number of dislocations n and a given value of τ_c, infinitely many combinations of d_g and τ_y can be found to produce equilibrium. There is a minimum d_g below which it is no longer possible to compress n dislocations in the pileup for a given tip stress τ_c. For any d_g larger than this value, the empty space in the centre of the grain will increase, but equilibrium can always be reached by compressing the DPU closer to the GB while maintaining $\tau_{Tip}=\tau_c$.

It is therefore necessary to find the minimal value of d_g, given n and τ_c, where the $n \times n$ nonlinear system no longer produces a valid solution. Invalid solutions have $x_1<0$ or, for very small d_g, do not converge. The lowest value of d_g, i.e., the smallest grain that can accommodate n dislocations under the condition that $\tau_{Tip}=\tau_c$ was used to establish the τ_y-d_g relationship.

To find this value, the theoretical value d_{th} for d_g was calculated using Eqs. (15) and (18), for a given value of n and τ_c. Equilibrium calculations were performed by varying d_g as a geometric sequence starting at d_{th} /4 in 36 steps with common ratio of $2^{1/8}$ for each value of n. Starting values for DPSD and DPCD are found from Eq. (16), using $A = \langle A \rangle$ for DPSD. For high values of d_g and n, convergence was sometimes not achieved, presumably because Eq. (16) does no longer provide reasonable starting values. The corresponding results were excluded. No further efforts were made to calculate the missing solutions because they are of little relevance for the analysis.

Numerical solvers available in the mathematical software are used to solve the system of $n \times n$ nonlinear equations. The sets of equations, variables and starting values are created automatically for any number of equations by user-defined routines. A maximum value of n=50 is used here, for reasons of convergence and computer time. A Newton solver with the trust region method for step control was used.

4.2. Numerical results

A comparison between the dislocation positions for SPID and SPSD with 50 dislocations is given in Fig. 6. The numerical simulations for the infinite dislocations coincide with the EFN-model, as expected. The positions for the continuous approximation are slightly different. Segment length has a strong effect. Shorter segments are spaced more closely, resulting in shorter pileups. A log-log plot of the τ_y-d_g relationship is given in Fig. 7. This way of presenting was chosen over the classical Hall-Petch plot because curves with different p are difficult to compare on a t_y vs. $d_g^{-1/2}$ plot.

The plot shows that a lower applied stress is needed to reach the critical tip stress when the segments are shorter. Fits to the curves for $2w=d_g$ and EFN yield k_{HP}=0.034 with p=0.42 and k_{HP}=0.063 with p=0.44, respectively. The experimental HP-constant for Cu is 0.118 as indicated in Section 2.1. The difference between these two curves highlights the considerable overestimation of stresses if infinite dislocations are used for modelling purposes.

Fig. 8 presents the results for the DPSD calculations for $2w=d_g$ in a log-log plot of τ_y vs. d_g, colour coded to distinguish n. Each

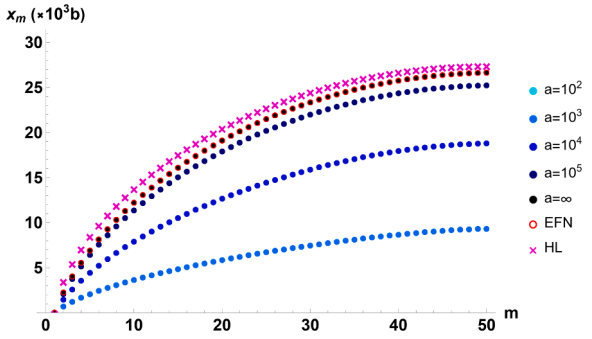

Fig. 6. Positions x_m (vertical axis, nondimensional) of dislocation n° m (m:2→50) in the pile-up for 5 different segment lengths, for the EFN-model and the continuum model (HL).

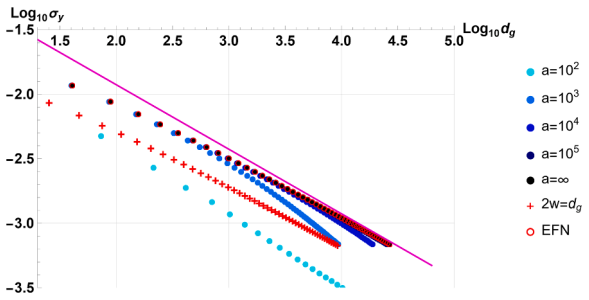

Fig. 7. Log-log plot of τ_y vs. d_g for 5 different segment lengths, for the EFN-model, and the simulations of short segments with length equal to the PU length; the straight line is the continuous approach. Non-dimensional units are used; considering the properties of Cu (Section 2.1), a value of 2 on the horizontal axis corresponds to 51 nm, −2 on the vertical axis corresponds to 581 MPa, an increase/decrease of one unit on the logarithmic axes corresponds to a multiplication/division by 10.

individual point corresponds to a valid solution out of the 1800 n-d_g combinations tested. The variation of τ_y with d_g for a given n is limited. The lower bound, representing the smallest grain that can accommodate n dislocations under the condition that $\tau_{Tip}=\tau_c$ is almost linear and corresponds to a nondimensional HP-constant of 0.050 and a HP-slope $p = 0.55$.

Fig. 9 shows the log-log plot of t_y vs. d_g for DPCD. Contrary to the former case, the values of t_y strongly depend on d_g. For each value of n, the results follow the lower bound curve for moderate values of d_g, resulting in considerable, but fully consistent overlap between the results for different n. Again, each dot represents a valid solution out of 1800 calculations. The lower bound no longer is a straight line, but if a linear approximation is made, a nondimensional HP-constant of 0.235 and slope $p = 0.61$ is found.

4.3. Slip and dislocation density

Early work on the elastic theory of dislocations tended to neglect the effects of dislocation slip. However, the creation of a pileup, of geometrically necessary dislocations (Ashby, 1970) or the increased density in the shell of core-shell models (Meyers et al., 2006) induces plastic shear, as the dislocations must travel from some source in the bulk or GB toward their final position in the pileup or GB-region. This strain (γ), and the associated dislocation density ρ_d, must be in reasonable agreement with observations. The calculation of these quantities is elaborated in the appendix.

Values for ρ_d are plotted in Fig. 10 and for γ in Fig. 11. Dimensional units are used in these images to facilitate comparison to commonly known values, with physical properties for Cu (Section 2.1) used in the calculations.

5. Discussion

5.1. Consistency of the models

Although alternative hypotheses (Section 1.1) are known to specialists in the area, there is a widespread acceptance in the materials science community that DPUs provide the explanation for the GSE. Under this hypothesis, quantitative comparison of the models can be made by using the experimentally determined value of the HP-constant to calculate the critical dislocation tip stress τ_c for yield.

EFN considers infinite straight dislocations, which cannot exist, given the geometry of the grains in a polycrystal. The continuum approach (Head and Louat, 1955) is a further simplification. Armstrong et al. (1966) have documented the significant difference

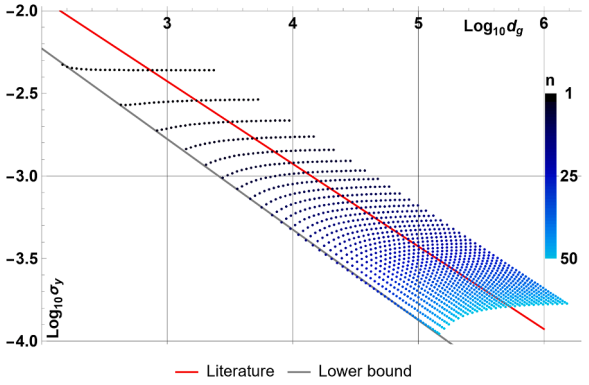

Fig. 8. Results of the DPSD calculations. Each series of points corresponds to a set of valid results for given n and τ_c with varying d_g and $2w = d_g$ (see Section 4.1). The colour code corresponds to n which is varied from 1 to 50 (top left to bottom right); 36 values of d_g were tested for each n.

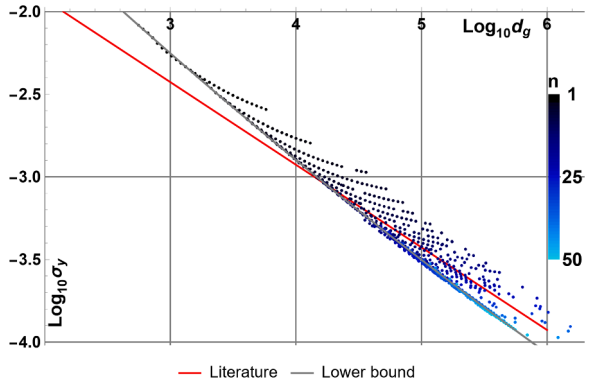

Fig. 9. Results of the DPCD calculations. Each series of point corresponds to a set of valid results for given n and τ_c with varying d_g (see Section 4.1). The colour code corresponds to n which is varied from 1 to 50 (top left to bottom right); 36 values of d_g were tested for each n.

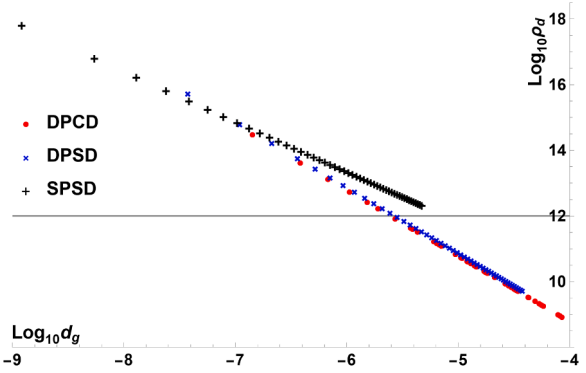

Fig. 10. Log-log plot of ρ_d vs d_g, with ρ_d the dislocation density required to produce a critical DPUs. Lengths are expressed in m, i.e., a value of −6 on the horizontal axis corresponds to 1μm, 12 on the vertical axis corresponds to $\rho_d = 10^{12}\text{m}^{-2}$, the commonly cited value for an undeformed material.

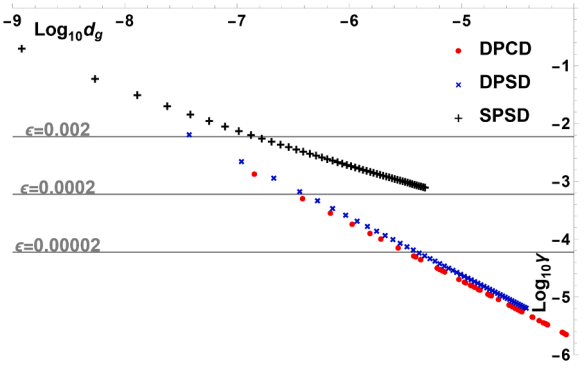

Fig. 11. Log-log plot of γ vs d_g, with γ the slip induced by the formation of critical DPUs. Lengths are expressed in m. Reference values of uniaxial strain ε=3γ are shown in grey.

between HL and EFN, but their analysis was limited to low values of n. The effect of using infinite dislocations has not been assessed in earlier work. Here, it is studied by using finite segments, which cannot exist either. Irradiation damage can create loops which are close to circular, but they do not pile up. A circular loop piling up at the GB would become polygonal. In presence of a dislocation forest, however dilute, the geometry can become very complex (Gil-Sevillano et al., 1991).

Simplified models are a valid means of studying complex phenomena, as long as various simplifications point toward the same results and can be verified experimentally. The inconsistency between the continuum models was already pointed out by Li and Chou (1970) and illustrated by the difference between Eqs. (10), (14) and (17), with $k_{SPID} = k_{DPID}/2 = k_{CPCD}/\pi$ (for $A = \langle A \rangle$). Fig. 7 shows that EFN approaches SPID only slowly, reaching convergence for d_g>25mm, which is not considered a small grain size. None of the

discrete models approach the continuum models for grain sizes up to 5μm, nor do they converge to each other. In general, it is seen that small changes in the model geometry (type of pileup, segment length) produce significant changes in the results. For DPSD and DPCD, the problem is not even uniquely defined: for any value of n, there exist infinitely many valid d_g-τ_c combinations. This lack of consistency is an argument against the validity of DPU-based models.

5.2. Power law relationships

The main argument for adopting PU-models has been that they predict a $d_g^{-1/2}$ relationship and that HP proposes a $d_g^{-1/2}$ relationship. Whether this is a valid scientific reasoning can be a point of discussion. Advanced statistical analysis of large datasets of experimental results indicates that the exponent $p \neq 1/2$. The numerical models presented here also do not show a $d_g^{-1/2}$ relationship. This removes the principal argument for a relationship between DPUs and HP.

It is tempting to point out that the simplified models predict a power law relationship between τ_c and d_g. Experimental values (Cordero et al., 2016) and numerical results (this work) are given in Table 1. Power laws can be used to fit a very wide range of datasets, even if the underlying mathematical equations do not support such a relationship. This is illustrated by EFN, which can be fitted to a power law in the range studied. Often, this involves biased observation. Here, only the continuum models are supported by a mathematical analysis, but they are inconsistent with results for discrete and finite dislocations.

It can be stated that the data in Table 1 are in reasonable agreement, but this is only apparent. Small changes in p induce large changes in $k_{HP} = 10^{\Delta y}$, with Δy the intersection on the vertical axis in the log-log plot. Modifying the assumptions about τ_c will modify k_{HP} but not p. Therefore, only p can be used to compare the values in Table 1. For FCC-materials, p corresponds more closely to SPSD; for BCC, DPSD produces a better approximation. Evidently, unless supported by strong experimental evidence, such discussion is non-scientific, as each alloy class would then have its own pileup geometry. The fact that both model and experiment can be fitted by d_g^{-p}-relationships is not an argument in favour of the DPU-hypothesis. However, it also does not allow to disprove the relationship between DPUs and the GSE.

5.3. Physical considerations

The calculated dislocation densities (Fig. 10) can be compared to experimental values. Hordon and Averbach (1961) used line profile analysis to estimate the dislocation density in Cu and Al. For the lowest strain levels investigated, they found values of 10^{12}m^{-2}. Mecking and Kocks (1981) compiled data for ρ_d in Cu deformed to different strain levels. The lowest densities in this reference are between 10^9 and 10^{10} m^{-2}. Jakobsen et al. (2007), using high angular resolution 3DXRD, reached the conclusion that $\rho_d < 10^{12}$ m^{-2} in Cu deformed to 2%.

For SPSD, ρ_d is above these minimum values for all d_g. For DPSD and DPCD, $\rho_d > 10^{12}$ m^{-2} is predicted as d_g drops below 1μm. On the other hand, for large d_g, the models predict that the strain involved in reaching this point is much smaller than the conventional 0.2% used to define the proof stress, as is common in most non-ferrous alloys. It shall be reminded that Petch (1953) studied the cleavage of steel and Hall (1951) studied the yield point, which are sudden and critical transitions from one type of behaviour to another. Then, the concept of a critical stress concentration which allows for the sudden propagation through the entire microstructure of a crack or plastic deformation can be valid. The yield point in iron and steel has since long been explained by an entirely different mechanism (Cottrell and Bilby, 1949). A sudden elastic-plastic transition is not observed in non-ferrous materials, which nonetheless show the GSE.

It can be proposed to attribute the gradual transition from elastic to plastic in tensile tests to the presence of differently orientated grains, with the resolved shear stress reaching its critical value over a certain range in the different grains. This topic has not been investigated into depth in relationship to DPUs, but it can be questioned whether the concept of sudden strain transmission from one grain to the other would still be relevant under this approach. This is a topic for future investigation.

The most problematic assumption in this context is the existence of a critical tip stress τ_c. Such value cannot be defined as a single constant. Both the character of the GBs and the misalignment between the slip systems depend on the misorientation between the grains (Shen et al., 1988; Clark et al., 1992.; Zhang et al., 2021), while the resolved shear stress on the slip systems depends on their orientation in the sample reference system. The claim of a direct relationship between DPUs and the GSE cannot be made without seriously considering this complexity.

5.4. Importance of DPUs

The main argument against DPUs as the explanation for the GSE is that they contradict the experimental observations (Bailey and

Table 1
Non-dimensional experimental and model values for k_{HP} and p in Eq. (1). (*) indicate data from Cordero et al. Two values of k_{HP} for Cu are given, one assuming $p = 1/2$ and the second one corresponding to a best fit to Eq. (1).

	Cu * $p = 1/2$	Cu * best fit	FCC *	BCC *	HCP *	EFN (d_g<25μm)	SPSD ($2w=d_g$)	DPSD ($2w=d_g$)	DPCD
k_{HP}	0.118	0.064				0.063	0.034	0.050	0.24
p	1/2	0.38	0.40±0.08	0.52±0.09	0.29±0.07	0.44	0.42	0.55	0.61

Hirsch, 1960) or that they are not universally observed, whereas the GSE is (Li and Chou, 1970; Saada, 2005). The present discussion points out the inconsistency of directly connecting DPUs to the GSE. This does not make the study of DPUs superfluous, as suggested by Li and Chou (1970).

Firstly, the stress fields calculated for the geometries studied here can be used for dislocation configurations which are not DPUs, as they are fully three-dimensional and applicable to any Burgers vector, including climb. The results are complex but can be handled with relative ease by introducing the Peach-Köhler formula in a systematic way in mathematical software. The corresponding software packages are annexed as supplementary information.

Secondly, DPUs do exist and interact with GBs in many interesting ways (Shen et al., 1988; Clark et al., 1992; Zhang et al., 2021; Bamney et al., 2022; Zhou et al., 2019; Murr, 2016; Zhao et al., 2020; Li et al., 2021; Liu et al., 2022a; Liu et al., 2022b; Britton and Wilkinson, 2012; Guo et al., 2014; Soer et al., 2004; De Hosson et al., 2006; Kondo et al., 2016; Piao and Khanh, 2021; Ruggles et al., 2020; Huang et al., 2019; Li et al., 2022). TEM observations do not allow to determine the length of dislocation segments in a bulk grain, but as the dislocation forest can be expected to be the main contributor for dislocations piling up at the GB (Mecking and Kocks, 1981; Gil-Sevillano et al., 1991; Schouwenaars, 2012), relatively short segments can be expected. It was found that short dislocations form shorter DPUs (Fig. 6) and reach the critical tip stress at lower values of the applied shear stress. This may explain why strain transmission across GBs occurs for relatively short DPUs in TEM-experiments.

Thirdly, the stress field of the short DPUs may offer an interesting tool for studying the relationship between DPUs, crystal orientation and GB misorientation mentioned in Section 5.3. Important progress has recently been made in this area using DDD (Jiang et al., 2019; Jiang et al. 2021; Zhang et al., 2021; Liu et al., 2022a; Liu et al., 2022b) and CPFEM (Demir and Gutierrez-Urrutia, 2021; Jiang et al., 2022; Zhang et al., 2022; Guan et al., 2022). These methods are computer intensive. While multiscale approaches can alleviate this problem (Peng et al., 2022; Lu et al., 2022a; Lu et al., 2022b) they still may pose problems for extensive parametric studies of dislocation behaviour at GBs.

The use of idealised dislocation configurations can simplify this task. A finite dislocation segment cannot exist within a crystal, but it may be more reasonable to accept the small stress concentrations at the ends of the segment (Fig. 2) than to induce other artifacts by using infinite dislocations. As the calculated stress field is fully 3-dimensional, it is possible to calculate DPUs in the grain, their interaction with the dissociation and climb of dislocations in the GB, and the resulting stress field in the neighbouring grain. The tensorial nature of the solutions allows the treatment of crystal orientation and misorientation through standard tensor transformations.

6. Summary and conclusions

The three-dimensional stress field of straight dislocation segments and circular loops with arbitrary Burgers vector were recalculated in tensorial form and made available in a user-friendly format. The results were used to compare the numerical solution of three dislocation pile-up models to the well-known continuum approximations for single, double, and circular pileups and the discrete Eshelby-Frank-Nabarro solution.

It was found that the singularities at the ends of finite dislocation segments are small, while infinite dislocations severely overestimate the magnitude of the stress field. The stress field of the circular dislocation loop is an interesting result by itself. The comparison between 4 theoretical and 3 numerical models reveals considerable inconsistencies in the pileup approach to the grain size effect.

The analysis of the single pileup shows that the length of the pileup is drastically reduced as the length of the segments is reduced and that the applied shear stress required to reach a critical tip stress is significantly lowered. Single pileups of finite dislocation segments may be a useful tool to study dislocation-grain boundary interactions into more detail.

None of the numerical results confirm the conventional $d_g^{-1/2}$ relationship. Extensive literature review indicates that such relationship is not firmly supported by experimental data either. This removes one of the principal arguments to associate the Hall-Petch relationship to dislocation pileups.

Although a d_g^{-p} relationship can be fitted to experimental GSE data and the DPS-models, no physical relationship can be established between the model geometry and experimental observation. Physical quantities, such as the dislocation density and amount of slip predicted by the DPU-models contradict experimental observation.

The concept of a critical tip stress, as a single value related to the Hall-Petch constant is inconsistent with the nature of dislocation transmission at grain boundaries. It neglects crystal orientation, grain boundary character and the misalignment of slip systems in neighbouring grains. Dislocation pileups certainly play a role in the plastic deformation of polycrystals through dislocation-grain boundary interaction, but they do not explain the grain size effect in a direct or consistent manner.

CRediT authorship contribution statement

R. Schouwenaars: Conceptualization, Methodology, Software, Validation, Formal analysis, Writing – original draft, Writing – review & editing. **L.A.I. Kestens:** Formal analysis, Writing – review & editing, Supervision, Project administration, Funding acquisition.

Declaration of Competing Interest

The authors declare that they have no known competing financial interests or personal relationships that could have appeared to influence the work reported in this paper.

Data availability

No data was used for the research described in the article.

Supplementary materials

Supplementary material associated with this article can be found, in the online version, at doi:10.1016/j.ijplas.2023.103602.

Appendix: plastic deformation and dislocation density associated to the formation of a DPU

The average strain gradient due to the slip of a single dislocation in a volume V, is found by homogenisation theory (Nemat-Nasser and Hori, 1999) as:

$$\overline{\nabla \mathbf{u}} = \frac{\mathbf{nb}\delta A}{V} \tag{A1}$$

with $\mathbf{n}$ the slip plane normal and dA the increase in slipped area. Taking the symmetrical part of $\overline{\nabla \mathbf{u}}$ and limiting Eq. (33) to simple slip in the shear plane, this reduces, in non-dimensional units, to:

$$\gamma = \frac{\delta A}{2V} \tag{A2}$$

For circular dislocation loops in a spherical grain, ρ_d is found by summing the circumference $2\pi x_i$ of the individual loops and dividing by the volume $4\pi r^3/3$ of a spherical grain, with $r=d_g/2$:

$$\rho_d = \frac{12}{d_g^3}\sum x_i \tag{A3}$$

Each loop expands from $A = 0$ to $A=\pi x_i^2$. Using Eq. (A1), assuming spherical grains and summing over all loops gives:

$$\gamma = \frac{3}{d_g^3}\sum x_i^2 \tag{A4}$$

For SPSD and DPSD, a cube-shaped grain is assumed with sides d_g. Assuming that the dislocation extends over the entire width of the grain ($2w=d_g$), the area dA affected by the slip of a single dislocation is equal to $d_g x_i$. For SPSD, it follows that:

$$\rho_d = \frac{n}{d_g^2} \tag{A5}$$

and:

$$\gamma = \frac{\sum x_i}{d_g^2} \tag{A6}$$

For DPSD, it must be reminded that, for each x_i, there are 2 dislocations and $2a=d_g$. Then:

$$\rho_d = \frac{2n}{d_g^2} \tag{A7}$$

and:

$$\gamma = \frac{2\sum x_i}{d_g^2} \tag{A8}$$

References

Akarapu, S., Hirth, J.P., 2013. Dislocation pile-ups in stress gradients revisited. Acta Mater. 61, 3621–3629. https://doi.org/10.1016/j.actamat.2013.02.049.

Aragon, N.K., Gravell, J.D., Ryu, I., 2022. Dislocation interactions at the grain boundary in FCC bicrystals: an atomistically-informed dislocation dynamics study. Acta Mater. 223, 117455 https://doi.org/10.1016/j.actamat.2021.117455.

Argon, A., 2007. Strengthening Mechanisms in Crystal Plasticity. OUP Oxford.

Ashby, M.F., 1970. The deformation of plastically non-homogeneous materials. Philos. Mag. A 21, 399–424. https://doi.org/10.1080/14786437008238426.

Armstrong, R.W., Chou, Y.T., Fisher, R.M., Louat, N., 1966. The limiting grain size dependence of the strength of a polycrystalline aggregate. Philos. Mag. 14, 943–951. https://doi.org/10.1080/14786436608244765.

Bailey, J.E., Hirsch, P.B., 1960. The dislocation distribution, flow stress, and stored energy in cold-worked polycrystalline silver. Philos. Mag. 5, 485–497. https://doi.org/10.1080/14786436008238300.

Bamney, D., Capolungo, L., Spearot, D.E., 2021. Role of equilibrium and non-equilibrium grain boundary stress fields on dislocation transmission. J. Mater. Res. 36, 2687–2704. https://doi.org/10.1557/s43578-021-00129-1.

Bamney, D., Reyes, R., Capolungo, L., Spearot, D.E., 2022. Disclination-dislocation based model for grain boundary stress field evolution due to slip transmission history and influence on subsequent dislocation transmission. J. Mech. Phys. Solids 165, 104920. https://doi.org/10.1016/j.jmps.2022.104920.

Baskaran, R., Akarapu, S., Mesarovic, S.D., Zbib, H.M., 2010. Energies and distributions of dislocations in stacked pile-ups. Int. J. Solids Struct. 47, 1144–1153. https://doi.org/10.1016/j.ijsolstr.2010.01.007.

Bayerschen, E., McBride, A.T., Reddy, B.D., Böhlke, T., 2016. Review on slip transmission criteria in experiments and crystal plasticity models. J. Mater. Sci. 51, 2243–2258. https://doi.org/10.1007/s10853-015-9553-4.

Berbenni, S., Taupin, V., Lebensohn, R.A., 2020. A fast Fourier transform-based mesoscale field dislocation mechanics study of grain size effects and reversible plasticity in polycrystals. J. Mech. Phys. Solids 135, 103808. https://doi.org/10.1016/j.jmps.2019.103808.

Bieler, T.R., Eisenlohr, P., Zhang, C., Phukan, H.J., Crimp, M.A., 2014. Grain boundaries and interfaces in slip transfer. Curr. Opin. Solid State Mater. Sci. 18, 212–226. https://doi.org/10.1016/j.cossms.2014.05.003.

Britton, T.B., Wilkinson, A.J., 2012. Stress fields and geometrically necessary dislocation density distributions near the head of a blocked slip band. Acta Mater. 60, 5773–5782. https://doi.org/10.1016/j.actamat.2012.07.004.

Chassagne, M., Legros, M., Rodney, D., 2011. Atomic-scale simulation of screw dislocation/coherent twin boundary interaction in Al, Au, Cu and Ni. Acta Mater. 59, 1456–1463. https://doi.org/10.1016/j.actamat.2010.11.007.

Chen, X., Richeton, T., Motz, C., Berbenni, S., 2019. Elastic fields due to dislocations in anisotropic bi-and tri-materials: applications to discrete dislocation pile-ups at grain boundaries. Int. J. Solids Struct. 164, 141–156. https://doi.org/10.1016/j.ijsolstr.2019.01.020.

Chen, X., Richeton, T., Motz, C., Berbenni, S., 2020. Atomic force microscopy study of discrete dislocation pile-ups at grain boundaries in Bi-crystalline micro-pillars. Crystals 10, 411. https://doi.org/10.3390/cryst10050411.

Chen, X., Richeton, T., Motz, C., Berbenni, S., 2021. Surface effects on image stresses and dislocation pile-ups in anisotropic bi-crystals. Int. J. Plast. 143, 102967 https://doi.org/10.1016/j.ijplas.2021.102967.

Chou, Y.T., 1967. Dislocation pile-ups against a locked dislocation of a different burgers vector. J. Appl. Phys. 38, 2080–2085. https://doi.org/10.1063/1.1709833.

Clark, W.A.T., Wagoner, R.H., Shen, Z.Y., Lee, T.C., Robertson, I.M., Birnbaum, H.K., 1992. On the criteria for slip transmission across interfaces in polycrystals. Scripta Metall. Mater. 26, 203–206. https://doi.org/10.1016/0956-716X(92)90173-C.

Conrad, H., 1963. Effect of grain size on the lower yield and flow stress of iron and steel. Acta Metall. 11 (1), 75–77. https://doi.org/10.1016/0001-6160(63)90134-2.

Cordero, Z.C., Knight, B.E., Schuh, C.A., 2016. Six decades of the Hall–Petch effect–a survey of grain-size strengthening studies on pure metals. Int. Mater. Rev. 61, 495–512. https://doi.org/10.1080/09506608.2016.1191808.

Cottrell, A.H., Bilby, B.A., 1949. Dislocation theory of yielding and strain ageing of iron. Proc. Phys. Soc. A 62, 49. https://doi.org/10.1088/0370-1298/62/1/308.

Demir, E., Gutierrez-Urrutia, I., 2021. Investigation of strain hardening near grain boundaries of an aluminum oligocrystal: experiments and crystal based finite element method. Int. J. Plast. 136, 102898 https://doi.org/10.1016/j.ijplas.2020.102898.

de Geus, T.W.J., Peerlings, R.H.J., Hirschberger, C.B., 2013. An analysis of the pile-up of infinite periodic walls of edge dislocations. Mech. Res. Comm. 54, 7–13. https://doi.org/10.1016/j.mechrescom.2013.08.010.

De Hosson, J.T., Soer, W.A., Minor, A.M., Shan, Z., Stach, E.A., Asif, S.S., Warren, O.L., 2006. *In situ* TEM nanoindentation and dislocation-grain boundary interactions: a tribute to David Brandon. J. Mater. Sci. 41, 7704–7719. https://doi.org/10.1007/s10853-006-0472-2.

Dunstan, D.J., Bushby, A.J., 2013. The scaling exponent in the size effect of small scale plastic deformation. Int. J. Plast. 40, 152–162. https://doi.org/10.1016/j.ijplas.2012.08.002.

Dunstan, D.J., Bushby, A.J., 2014. Grain size dependence of the strength of metals: the Hall–Petch effect does not scale as the inverse square root of grain size. Int. J. Plast. 53, 56–65. https://doi.org/10.1016/j.ijplas.2013.07.004.

El-Awady, J.A., 2015. Unravelling the physics of size-dependent dislocation-mediated plasticity. Nat. Comm. 6, 1–9. https://doi.org/10.1038/ncomms6926.

Eshelby, J.D., Frank, F.C., Nabarro, F.R.N., 1951. The equilibrium of linear arrays of dislocations. Philos. Mag. 42. https://doi.org/10.1080/14786445108561060.

Foreman, A.J.E., 1967. The bowing of a dislocation segment. Philos. Mag. 15, 1011–1021. https://doi.org/10.1080/14786436708221645.

Friedman, L.H., Chrzan, D.C., 1998. Continuum analysis of dislocation pile-ups: influence of sources. Philos. Mag. A 77, 1185–1204. https://doi.org/10.1080/01418619808214247.

Gil-Sevillano, J., Bouchaud, E., Kubin, L.P., 1991. The fractal nature of gliding dislocation lines. Scr. Metall. Mater. 25, 355–360. https://doi.org/10.1016/0956-716X(91)90192-4.

Gu, Y., Eastman, D.W., Hemker, K.J., El-Awady, J.A., 2021. A statistical model for predicting size effects on the yield strength in dislocation-mediated crystal plasticity. J. Mech. Phys. Solids 147, 104245. https://doi.org/10.1016/j.jmps.2020.104245.

Guan, B., Xin, Y., Huang, X., Wu, P., Liu, Q., 2019. Quantitative prediction of texture effect on Hall–Petch slope for magnesium alloys. Acta Mater. 173, 142–152. https://doi.org/10.1016/j.actamat.2019.05.016.

Guan, B., Xin, Y., Huang, X., Liu, C., Wu, P., Liu, Q., 2022. The mechanism for an orientation dependence of grain boundary strengthening in pure titanium. Int. J. Plast. 153, 103276 https://doi.org/10.1016/j.ijplas.2022.103276.

Guo, Y., Britton, T.B., Wilkinson, A.J., 2014. Slip band–grain boundary interactions in commercial-purity titanium. Acta Mater. 76, 1–12. https://doi.org/10.1016/j.actamat.2014.05.015.

Hall, E.O., 1951. The deformation and ageing of mild steel: III Discussion of results. Proc. R. Soc. B64 https://doi.org/10.1088/0370-1301/64/9/303, 747-735.

Head, A.K., Louat, N., 1955. The distribution of dislocations in linear arrays. Austr. J. Phys. 8, 1–7. https://doi.org/10.1071/PH550001.

Hirth, J.P., Lothe, J., 1992. Theory of Dislocations. Krieger Publishing Co. Florida.

Hordon, M.J., Averbach, B.L., 1961. X-ray measurements of dislocation density in deformed copper and aluminum single crystals. Acta Metall. 9, 237–246. https://doi.org/10.1016/0001-6160(61)90073-6.

Huang, Z., Yang, C., Qi, L., Allison, J.E., Misra, A., 2019. Dislocation pile-ups at β1 precipitate interfaces in Mg-rare earth (RE) alloys. Mater. Sci. Eng. A 742, 278–286. https://doi.org/10.1016/j.msea.2018.10.104.

Jakobsen, B., Poulsen, H.F., Lienert, U., Pantleon, W., 2007. Direct determination of elastic strains and dislocation densities in individual subgrains in deformation structures. Acta Mater. 55, 3421–3430. https://doi.org/10.1016/j.actamat.2007.01.049.

Ji, R., Phan, T., Chen, H., Xiong, L., 2020. Quantifying the dynamics of dislocation kinks in iron and tungsten through atomistic simulations. Int. J. Plast. 128, 102675 https://doi.org/10.1016/j.ijplas.2020.102675.

Ji, R., Phan, T., Chen, Y., McDowell, D.L., Xiong, L., 2022. A finite-temperature coarse-grained atomistic approach for understanding the kink-controlled dynamics of micrometer-long dislocations in high-Peierls-barrier materials. MRS Commun. 1–9. https://doi.org/10.1557/s43579-022-00238-w.

Jiang, M., Devincre, B., Monnet, G., 2019. Effects of the grain size and shape on the flow stress: a dislocation dynamics study. Int. J. Plast. 113, 111–124. https://doi.org/10.1016/j.ijplas.2018.09.008.
Jiang, M., Monnet, G., Devincre, B., 2021. On the origin of the Hall–Petch law: a 3D-dislocation dynamics simulation investigation. Acta Mater. 209, 116783 https://doi.org/10.1016/j.actamat.2021.116783.
Jiang, M., Fan, Z., Kruch, S., Devincre, B., 2022. Grain size effect of FCC polycrystal: a new CPFEM approach based on surface geometrically necessary dislocations. Int. J. Plast. 103181 https://doi.org/10.1016/j.ijplas.2021.103181.
Kacher, J., Eftink, B.P., Cui, B., Robertson, I.M., 2014. Dislocation interactions with grain boundaries. Curr. Opin. Solid State Mater. Sci. 18, 227–243. https://doi.org/10.1016/j.cossms.2014.05.004.
Kalaei, A., Xiang, Y., Ngan, A.H., 2022. An efficient and minimalist scheme for continuum dislocation dynamics. Int. J. Plast. 158, 103433 https://doi.org/10.1016/j.ijplas.2022.103433.
Kato, M., Fujii, T., Onaka, S., 2008. Dislocation bow-out model for yield stress of ultra-fine grained materials. Mater. Trans. 49, 1278–1283. https://doi.org/10.2320/matertrans.MRA2008012.
Khraishi, T.A., Hirth, J.P., Zbib, H.M., Khaleel, M.A., 2000a. The displacement, and strain–stress fields of a general circular Volterra dislocation loop. Int. J. Eng. Sci. 38, 251–266. https://doi.org/10.1016/S0020-7225(99)00038-5.
Khraishi, T.A., Hirth, J.P., Zbib, H.M., De La Rubia, T.D., 2000b. The stress field of a general circular Volterra dislocation loop: analytical and numerical approaches. Philos. Mag. Lett. 80, 95–105. https://doi.org/10.1080/095008300176353.
Kondo, S., Mitsuma, T., Shibata, N., Ikuhara, Y., 2016. Direct observation of individual dislocation interaction processes with grain boundaries. Sci. Adv. 2, e1501926 https://doi.org/10.1126/sciadv.1501926.
Kroupa, F., 1961. The force between non-parallel dislocations. Czech. J. Phys. 11, 847–848. https://doi.org/10.1007/BF01690051.
Leibfried, G., 1951. Verteilung von Versetzungen im statischen Gleichgewicht. Z. Phys. 130, 214–226. https://doi.org/10.1007/BF01337695.
Li, Y., Bushby, A.J., Dunstan, D.J., 2016. The Hall–Petch effect as a manifestation of the general size effect. Proc. R. Soc. A 472, 20150890. https://doi.org/10.1098/rspa.2015.0890.
Li, J.C., Liu, G.C., 1967. Circular dislocation pile-ups: I. Strength of ultra-fine polycrystalline aggregates. Philos. Mag. 15, 1059–1063. https://doi.org/10.1080/14786436708221653.
Li, J.C.M., Feng, C.R., Rath, B.B., 2020. Emission of dislocations from grain boundaries and its role in nanomaterials. Crystals 11, 41–42. https://doi.org/10.3390/cryst11010041.
Li, J.C.M., Chou, Y.T., 1970. The role of dislocations in the flow stress grain size relationships. Metall. Mater. Trans. B 1, 1145–1159. https://doi.org/10.1007/BF02900225.
Li, X., Holdsworth, S.R., Kalácska, S., Balogh, L., Park, J.S., Dasilva, Y.A.R., Maeder, X., Cocks, A., Mazza, E., Hosseini, E., 2021. *In-situ* and *ex-situ* microstructure studies and dislocation-based modelling for primary creep regeneration response of 316H stainless steel. Acta Mater. 216, 117130 https://doi.org/10.1016/j.actamat.2021.117130.
Li, Z., Zhang, J., Zhai, Y., Zhang, J., Wang, X., Zhang, Z., Mao, S., Han, X., 2022. Dynamic mechanisms of strengthening and softening of coherent twin boundary via dislocation pile-up and cross-slip. Mater. Res. Lett. 10, 539–546. https://doi.org/10.1080/21663831.2022.2065892.
Liu, C., Zhang, J., Yang, Y., Xia, X., He, T., Ding, J., Tang, Y., Zhang, Z., Chen, X., Liu, Y., 2022a. Hot deformation behavior of ATI 718Plus alloy with different microstructures. Acta Metall. Sin. (Engl. Lett.) 35, 1383–1396. https://doi.org/10.1007/s40195-021-01361-8.
Liu, W., Liu, Y., Sui, H., Chen, L., Yu, L., Yi, X., Duan, H., 2020. Dislocation-grain boundary interaction in metallic materials: competition between dislocation transmission and dislocation source activation. J. Mech. Phys. Solids 145, 104158. https://doi.org/10.1016/j.jmps.2020.104158.
Liu, W., Yu, L., Liu, Y., Sui, H., Fan, H., Duan, H., 2022b. Dislocation pile-up polarization model for mechanical properties of polycrystalline metals based on grain boundary resistance variability. J. Mech. Phys. Solids 160, 104793. https://doi.org/10.1016/j.jmps.2022.104793.
Lu, S., Kan, Q., Zaiser, M., Li, Z., Kang, G., Zhang, X., 2022a. Size-dependent yield stress in ultrafine-grained polycrystals: a multiscale discrete dislocation dynamics study. Int. J. Plast. 149, 103183 https://doi.org/10.1016/j.ijplas.2021.103183.
Lu, S., Zhao, J., Huang, M., Li, Z., Kang, G., Zhang, X., 2022b. Multiscale discrete dislocation dynamics study of gradient nano-grained materials. Int. J. Plast., 103356 https://doi.org/10.1016/j.ijplas.2022.103356.
Mecking, H., Kocks, U.F., 1981. Kinetics of flow and strain-hardening. Acta Metall. 29, 1865–1875. https://doi.org/10.1016/0001-6160(81)90112-7.
Meyers, M.A., Mishra, A., Benson, D.J., 2006. Mechanical properties of nanocrystalline materials. Prog. Mater. Sci. 51, 427–556. https://doi.org/10.1016/j.pmatsci.2005.08.003.
Murr, L.E., 2016. Dislocation ledge sources: dispelling the myth of Frank–Read source importance. Metall. Mater. Trans. A 47, 5811–5826. https://doi.org/10.1007/s11661-015-3286-5.
Nemat Nasser, S., Hori, M., 1999. Micromechanics: Overall properties of Heterogeneous Materials. Elsevier, Amsterdam.
Orowan, E., 1940. Problems of plastic gliding. Proc. Phys. Soc. 52, 8–22. https://doi.org/10.1088/0959-5309/52/1/303.
Ovid'Ko, I.A., Valiev, R.Z., Zhu, Y.T., 2018. Review on superior strength and enhanced ductility of metallic nanomaterials. Prog. Mater. Sci. 94, 462–540. https://doi.org/10.1016/j.pmatsci.2018.02.002.
Pai, N., Prakash, A., Samajdar, I., Patra, A., 2022. Study of grain boundary orientation gradients through combined experiments and strain gradient crystal plasticity modeling. Int. J. Plast. 156, 103360 https://doi.org/10.1016/j.ijplas.2022.103360.
Peach, M., Koehler, J., 1950. The forces exerted on dislocations and the stress fields produced by them. Phys. Rev. 80, 436. https://doi.org/10.1103/PhysRev.80.436.
Peng, Y., Ji, R., Phan, T., Gao, W., Levitas, V.I., Xiong, L., 2022. An atomistic-to-microscale computational analysis of the dislocation pileup-induced local stresses near an interface in plastically deformed two-phase materials. Acta Mater. 226, 117663 https://doi.org/10.1016/j.actamat.2022.117663.
Perevezentsev, V.N., Kirikov, S.V., Svirina, Y.V., 2020. Conditions of strain-induced facet formation during interaction between a lattice dislocation pile-up and a grain boundary. Phys. Met. Metall. 121, 929–935. https://doi.org/10.1134/S0031918X20100087.
Petch, N.J., 1953. The cleavage strength of polycrystals. J. Iron Steel Inst. 174, 25–28.
Piao, Y., Le, K.C., 2021. Dislocation impediment by the grain boundaries in polycrystals. Acta Mech. 232 (8), 3193–3213. https://doi.org/10.1007/s00707-021-03007-3.
Roy, A., Peerlings, R.H.J., Geers, M.G.D., Kasyanyuk, Y., 2008. Continuum modeling of dislocation interactions: why discreteness matters? Mater. Sci. Eng. A 486, 653–661. https://doi.org/10.1016/j.msea.2007.09.074.
Ruggles, T.J., Yoo, Y.S.J., Dunlap, B.E., Crimp, M.A., Kacher, J., 2020. Correlating results from high resolution EBSD with TEM-and ECCI-based dislocation microscopy: approaching single dislocation sensitivity via noise reduction. Ultramicroscopy 210, 112927. https://doi.org/10.1016/j.ultramic.2019.112927.
Rybin, V.V., Perevezentsev, V.N., Svirina, Y.V., 2018. Analysis of the stability conditions for a dislocation pile-up hindered by the wedge disclination elastic field. Tech. Phys. 63, 974–978. https://doi.org/10.1134/S1063784218070241.
Saada, G., 2005. Hall–Petch revisited. Mater. Sci. Eng. A 400, 146–149. https://doi.org/10.1016/j.msea.2005.02.091.
Scardia, L., Peerlings, R.H., Peletier, M.A., Geers, M.G., 2014. Mechanics of dislocation pile-ups: a unification of scaling regimes. J. Mech. Phys. Solids 70, 42–61. https://doi.org/10.1016/j.jmps.2014.04.014.
Schouwenaars, R., 2020. Self-energy, line tension and bow-out of grain boundary dislocation sources. Int. J. Plast. 133, 102802 https://doi.org/10.1016/j.ijplas.2020.102802.
Schouwenaars, R., 2012. A statistical analysis of strain hardening: the percolation limit and the Taylor equation. Acta Mater. 60, 6331–6340. https://doi.org/10.1016/j.actamat.2012.08.008.
Schouwenaars, R., Seefeldt, M., Van Houtte, P., 2010. The stress field of an array of parallel dislocation pile-ups: implications for grain boundary hardening and excess dislocation distributions. Acta Mater. 58, 4344–4353. https://doi.org/10.1016/j.actamat.2010.04.026.
Shen, Z., Wagoner, R.H., Clark, W.A.T., 1988. Dislocation and grain boundary interactions in metals. Acta Met. 36, 3231–3242. https://doi.org/10.1016/0001-6160(88)90058-2.

Soer, W.A., De Hosson, J.T.M., Minor, A.M., Morris Jr, J.W., Stach, E.A., 2004. Effects of solute Mg on grain boundary and dislocation dynamics during nanoindentation of Al–Mg thin films. Acta Mater. 52, 5783–5790. https://doi.org/10.1016/j.actamat.2004.08.032.

Szajewski, B.A., Chakravarthy, S.S., Curtin, W.A., 2013. Operation of a 3D Frank–Read source in a stress gradient and implications for size-dependent plasticity. Acta Mater. 61, 1469–1477. https://doi.org/10.1016/j.actamat.2012.11.023.

Taylor, G.I., 1934. The mechanism of plastic deformation of crystals. Part I.—Theoretical. Proc. R. Soc. A 145, 362–387. https://www.jstor.org/stable/2935509.

Varin, R.A., Kurzydlowski, K.J., Tangri, K., 1987. Analytical treatment of grain boundary sources for dislocations. Mater. Sci. Eng. 85, 115–126. https://doi.org/10.1016/0025-5416(87)90473-3.

Wagoner, R.H., 1981. Calculating dislocation spacings in pile-ups at grain boundaries. Metall. Trans. A. 12, 2015–2023. https://doi.org/10.1007/BF02644170.

Yuan, R., Beyerlein, I.J., Zhou, C., 2015. Emergence of grain-size effects in nanocrystalline metals from statistical activation of discrete dislocation sources. Acta Mater. 90, 169–181. https://doi.org/10.1016/j.actamat.2015.02.035.

Yuan, R., Beyerlein, I.J., Zhou, C., 2016. Statistical dislocation activation from grain boundaries and its role in the plastic anisotropy of nanotwinned copper. Acta Mater. 110, 8–18. https://doi.org/10.1016/j.actamat.2016.02.064.

Zamani, Z., Shishvan, S.S., Assempour, A., 2015. Effect of source strength on dislocation pileups in the presence of stress gradients. Philos. Mag. 95, 2175–2197. https://doi.org/10.1080/14786435.2015.1054913.

Zhang, M., Rao, Z., Xu, T., Fang, L., 2020. Quantifying the influence of grain boundary activities on Hall-Petch relation in nanocrystalline Cu by using phase field and atomistic simulations. Int. J. Plast. 135, 102846.

Zhang, R., Xu, Z., Peng, L., Lai, X., Fu, M.W., 2022. Intragranularly misoriented grain boundary evolution affected by local constraints and grain size in micro-scale deformation of ultra-thin metallic sheets. Int. J. Plast. 157, 103377 https://doi.org/10.1016/j.ijplas.2022.103377.

Zhang, X., Hattar, K., Chen, Y., Shao, L., Li, J., Sun, C., Yu, K., Li, N., Taheri, M.L., Wang, H., Wang, J., 2018. Radiation damage in nanostructured materials. Prog. Mater. Sci. 96, 217–321. https://doi.org/10.1016/j.pmatsci.2018.03.002.

Zhang, X., Lu, S., Zhang, B., Tian, X., Kan, Q., Kang, G., 2021. Dislocation–grain boundary interaction-based discrete dislocation dynamics modeling and its application to bicrystals with different misorientations. Acta Mater. 202, 88–98. https://doi.org/10.1016/j.actamat.2020.10.052.

Zhao, Y., Li, K., Gargani, M., Xiong, W., 2020. A comparative analysis of Inconel 718 made by additive manufacturing and suction casting: microstructure evolution in homogenization. Addit. Manuf. 36, 101404 https://doi.org/10.1016/j.addma.2020.101404.

Zheng, Z., Waheed, S., Balint, D.S., Dunne, F.P., 2018. Slip transfer across phase boundaries in dual phase titanium alloys and the effect on strain rate sensitivity. Int. J. Plast. 104, 23–38. https://doi.org/10.1016/j.ijplas.2018.01.011.

Zhou, H., Huang, C., Sha, X., Xiao, L., Ma, X., Höppel, H.W., Göken, M., Wu, X., Ameyama, K., Han, X., Zhu, Y., 2019. *In-situ* observation of dislocation dynamics near heterostructured interfaces. Mater. Res. Lett. 7, 376–382. https://doi.org/10.1080/21663831.2019.1616330.